Dalton Transactions

ROYAL SOCIETY OF CHEMISTRY

PAPER

View Article Online
View Journal | View Issue

Cite this: *Dalton Trans.*, 2024, **53**, 564

Computation of ^{31}P NMR chemical shifts in Keggin–based lacunary polyoxotungstates†

Jake A. Thompson and Laia Vilà-Nadal *

Density Functional Theory (DFT) calculations were employed to systematically study the accuracy of various exchange-correlation functionals in reproducing experimental ^{31}P NMR chemical shifts, $\delta_{Exp}(^{31}P)$ for Keggin, $[PW_{12}O_{40}]^{3-}$ and corresponding lacunary clusters: $[PW_{11}O_{39}]^{7-}$, $[A\text{-}PW_9O_{34}]^{9-}$, and $[B\text{-}PW_9O_{34}]^{9-}$. Initially, computed chemical shifts, $\delta_{Calc}(^{31}P)$ were obtained with without neutralising their charge in which associated error, $\delta_{Error}(^{31}P)$, decreased as a function of Hartree–Fock (HF) exchange, attributed to constriction of the P–O tetrahedron. By comparison, $\delta_{Calc}(^{31}P)$ performed with explicitly located counterions to render the system charge neutral, reduced discrepancies, $\delta_{Error}(^{31}P)$ by 1–2 ppm. However, uncertainties in $\delta_{Calc}(^{31}P)$ remain, particularly for $[B\text{-}PW_9O_{34}]^{9-}$ anions attributed to direct electrostatic interactions between the counterions and the central tetrahedron. Optimal results were achieved using the PBE/TZP//PBE0/TZP method, achieving a mean absolute error (MAE) and a mean squared error (MSE) of 4.03 ppm. Our results emphasize that understanding the nature of the electrolyte and solvent environment is essential to obtaining reasonable agreement between theoretical and experimental results.

Received 18th August 2023,
Accepted 13th November 2023

DOI: 10.1039/d3dt02694a

rsc.li/dalton

Introduction

Polyoxometalates (POMs) are a large group of discrete, polynuclear metal–oxo clusters comprised of early transition-metal (addenda) and oxide atoms.[1–6] Addenda atoms are fully oxidized to d^0 electron configurations capable of forming various topologies employing $\{MO_x\}$ as the principal building block.[1–6] Polyoxo clusters are formed from the one-pot acidification of aqueous molybdate or tungstate oxoanions.[6–8] Self-assembly can be controlled by several synthetic variables including but not limited to: (i) concentration/type of metal oxide anion; (ii) pH and type of acid; (iii) presence of reducing agent; (iv) heteroatom concentration; (v) and solvent.[6–10] The synthesis and self-assembly mechanism of POMs requires a complex network of interdependent reactions, in which any slight variation to the listed five experimental variables can change the dominant species of the combinatorial library. Hence the outcome is often hard to predict.[11] Recent work exploiting the self-assembly properties of POMs with non-ionic organic matter was employed to enhance the structural and functional diversity of cyclodextrin-based open frameworks.[12]

Partial hydrolysis of poly-oxo clusters is achieved through the controlled addition of base produces lacunary clusters[9,10] Lacunary clusters formally 'lose' one or several M=O vertices and possess reactive cavities with high charge density around the defective region due to the negatively charged oxygen ligands.[13–17] The defect can react with transition-metal cations forming a new class of compounds, an example shown are mono-transition-metal-substituted polyoxotungstates posessing the general formula $[XW_{11}M(L)O_{39}]^{q-}$ (X = *e.g.* P(v), Si(iv), L = H_2O, DMSO, *etc.*).[13–18]

Nuclear magnetic resonance (NMR) of active nuclei has been routinely employed for characterising molecular structures in solution and solid state.[19] The employment of ^{1}H, ^{29}Si, and ^{31}P nuclei are common, producing resonance signals across a wide range of chemical shifts providing direct information of the chemical environment. For some cases, poorly sensitive nuclei (^{17}O, ^{183}W) require high concentrations ($\geq$ 0.1 M) coupled with long acquisition times.[19] By contrast, ^{31}P is a highly sensitive nucleus with 100% abundance, requiring significantly lower acquisition time and concentrations (< 0.01 M).[19] This spectroscopy provides structural information reflecting in the range of −350 to 300 ppm, relative to 85% H_3PO_4. A fundamental variable of POM chemistry is controlling solubility achieved through the incorporation of inorganic and organic counterions.[9] Their tuneable solubility in aqueous and organic media makes them suitable precursors for ^{31}P NMR investigations.[9] For decades, ^{31}P NMR has been used to identify intermediates to understand self-assembly mechanisms in

School of Chemistry, University of Glasgow, UK.
E-mail: laia.vila-nadal@chem.gla.ac.uk

†Electronic supplementary information (ESI) available: Selected structural parameters for Keggin, $[PW_{12}O_{40}]^{3-}$ and corresponding lacunary: $[PW_{11}O_{39}]^{7-}$, $[A\text{-}PW_9O_{34}]^{9-}$, and $[B\text{-}PW_9O_{34}]^{9-}$ clusters. Experimental ^{31}P NMR, IR, UV, and ESI-MS spectra. See DOI: https://doi.org/10.1039/d3dt02694a

POMs,[20] for example, the base degradation of $H_3PW_{12}O_{40}$ and the formation of high-nuclearity clusters such as $[P_8W_{48}O_{184}]^{40-}$ wheels.[20,21]

Early computational work in POMs has primarily focused on charged systems without implicit solvation models; see Fig. 1, in which we summarise the insights gained over the past 20-years regarding computed chemical shifts in POMs. In 2002, Bagno and co-workers calculated ^{99}Ru chemical shifts in $[PW_{11}Ru(DMSO)O_{39}]^{5-}$ without accounting for counterions, solvation, relativistic corrections.[22] The authors shown that shortening of *d*(Ru–S) by 0.045 Å induced shielding of the ^{99}Ru nucleus by 235 ppm.[22] These approximations produced results that were significantly underestimated with respect to experimental ^{99}Ru chemical shifts, obtained at 7737 ppm.[23] Later, Bagno and co-workers computed ^{183}W NMR signals in $[W_5O_{18}]^{6-}$, $[Ru(DMSO)PW_{11}O_{39}]^{5-}$, and $[PW_{11}O_{39}]^{7-}$ clusters accounting for relativistic effects using zero-order regular scalar approximations.[23] The authors reported the computed W1–W5 signals were deshielded relative to W6; only W2 and W3 reproduced trends shown by experimental work.[23] Counterion dependence of approx. 53 ppm was accounted for modelling with the $[LiPW_{11}O_{39}]^{6-}$ adduct.[23] The adduct demonstrated improved ordering of the signals, however, such chemical shifts did not accurately reproduce experimental work. Later, Bagno reported that incorporation of spin–orbit (SO) corrections, coupled with implicit solvation, provided optimal (average) accuracy for ^{183}W chemical shifts, determined at 35 ppm.[23] In 2009, Kortz and co-workers performed relativistic ^{183}W NMR calculations for the mono-lacunary clusters, $[GeW_{10}X(H_2O)O_{36}]^{7-}$ (X^+ = Li, Na, K) which incorporated counterions with explicitly located water.[24] The ordering of three resonances in $[GeW_{10}K(H_2O)O_{36}]^{7-}$ was successfully reproduced; although slightly shielded, replicated the experimental distance between W(B) and W(C) signals ($\Delta\delta$ = 26 ppm *vs.* 29 ppm).[24] The influence of counterions was shown by $\Delta\delta$ which was reduced to 19 ppm for $[GeW_{10}O_{36}]^{8-}$ systems.[24] Vilà-Nadal and co-workers rationalised these observations in $[XW_{12}O_{40}]^{q-}$ (X = B, Al, Si, P, Ga, Ge, As, Zn) by showing ^{183}W chemical shifts were linearly correlated with the tungsten-bridging oxygen (O_b and O_c) bond distances.[25] The authors proposed that the contraction of the WO_6 polyhedral increased the energy gap between the occupied and unoccupied orbitals involved in electronic transition, hence, the principal contribution to paramagnetic shielding, U_{ai}, becomes less negative, deshielding the nucleus.[25]

Linear scaling has been employed to reduce mean absolute error (MAE) of computed chemical shifts. In 2014, Pascual-Borràs and co-workers calculated ^{17}O chemical shifts for $[W_6O_{19}]^{2-}$ including spin–orbit corrections and implicit solvation providing an average mean absolute error of 39 ppm.[26] By incorporating scaling corrections, MAE was reduced to approx. 26 ppm across 75 signals.[26] Later, Pascual-Borràs and co-workers calculated ^{31}P chemical shifts in Keggin, $[PW_{12}O_{40}]^{3-}$, and Wells–Dawson, $[P_2W_{18}O_{62}]^{6-}$ anions reporting MAE values of 2.62 ppm. The authors performed a systematic benchmark employing several exchange–correaltion *(x-c)* functionals and concluded that the optimal methodology was TZP/PBE//TZ2P/OPBE (NMR//optimization step)coupled with spin–orbit (SO) corrections and implicit solvation. Linear scaling corrections were applied which further reduced MAE to 0.57 ppm.[27] The authors rationalised chemical shifts with orbital gaps as an approximation to the probability of electronic transition. For example, chemical shifts became more positive as a function of metal oxidation state (X = W(VI) > V(V) > Sn(IV) > Ru(II)) in $[P_2W_{17}M(H_2O)O_{61}]^{q-}$ anions.[27]

Contemporary quantum chemical calculations have focused on charged systems with spin–orbit (SO) corrections and implicit solvation models. Obtaining accurate models for computing ^{31}P chemical shifts is crucial for spectral assignments of experimental data. The role of counterions in computed ^{31}P chemical shifts have not been throughly investigated. DFT calculations currently rely on linear scaling to obtain sufficiently accurate results requiring a significant number of calculations to generate these regression models. In this work, we have employed density functional theory (DFT) calculations to reproduce experimental ^{31}P NMR shifts in Keggin and corresponding mono- and tri-lacunary clusters, see Fig. 2. The present work will assess the accuracy of various exchange-correlation functionals and applied basis sets in reproducing experimental ^{31}P NMR chemical shifts and provide a detailed analysis on the effect of the geomtric factors controlling it.

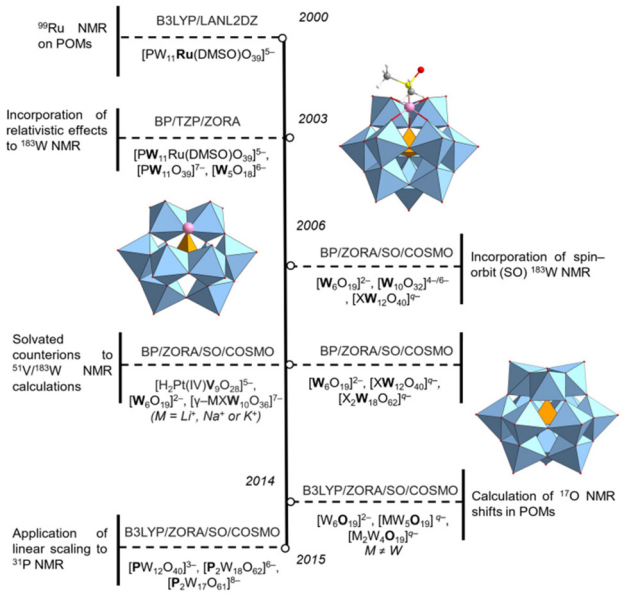

Fig. 1 Timeline showing the progression of NMR calculations in polyoxometalates.[22–29]

Experimental

Materials and methods

All reagents and solvents were supplied by Sigma Aldrich Chemical Company Ltd, Thermo Fisher Scientific, and

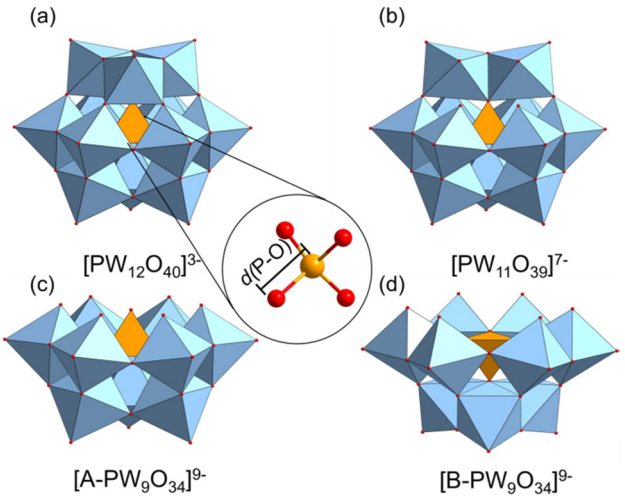

Fig. 2 Polyhedral representations of the hydrolytic conversions of $[PW_{12}O_{40}]^{3-}$ to lacunary: $[PW_{11}O_{39}]^{7-}$, $[A\text{-}PW_9O_{34}]^{9-}$, and $[B\text{-}PW_9O_{34}]^{9-}$ clusters. Colours corresponding to W = cyan, O = red, and P = orange.

Cambridge Isotope Laboratories. All materials were used without further purification.

FT-IR spectra were recorded on a Nicolet 170SX-FT/IR spectrometer in the range of 400–4000 cm^{-1}. **UV-Vis** spectra of the prepared compounds were measured in the region (200–400) nm for 30 μM solutions in distilled water at 25 °C using a Shimadzu 1800 spectrophotometer matched quartz cell. All **^{31}P NMR** spectroscopy was performed using a Bruker DPX 400 spectrometer with 85% phosphoric acid as an external standard. All spectra were recorded using 50 mg samples dissolved in D_2O. All tetrabutylammonium (TBA) salts were recorded using 50 mg samples dissolved in CD_3CN. Electrospray ionization mass spectrometry (**ESI-MS**) was obtained in negative-ion mode on the Agilent Q-TOF 6520 LC/MS mass spectrometer. The electrospray ionization source conditions: V_{cap}, 3500 V; skimmer, 65 V; nebulizer, 30 psi; drying and nebulizer gas, N_2; drying gas flow, 10 L min^{-1}; drying gas temperature, 300 °C; fragmentor, 80 V; scan range 100–2000 *m*/*z*. The sample solutions with the concentration of approximately 1000 ppm were made and analysed by direct injection using an automatic sampler with a flow rate of 0.2 mL min^{-1}.

Preparation

Preparation of $Li_3[PW_{12}O_{40}]$. This was prepared in accordance with the literature.[28] Phosphotungstic acid hydrate (5.0 g, 1.74 mmol) was dissolved in water (20 mL). LiCl (0.22 g, 5.21 mmol) was dissolved in the phosphotungstic solution, under stirring for 1 h. The solvent was evaporated off at 373 K producing a white crystalline powder (5.05 g, 98.6%).

Preparation of $Na_3[PW_{12}O_{40}]$. This was prepared in accordance with the literature.[28] Phosphotungstic acid hydrate (5.0 g, 1.74 mmol) was dissolved in water (20 mL). NaCl (0.10 g, 5.21 mmol) was dissolved in the phosphotungstic solution, under stirring for 1 h. The solvent was evaporated off at 373 K producing a white crystalline powder (4.97 g, 98.6%).

Preparation of $[(n\text{-}C_4H_9)_4N]_3[PW_{12}O_{40}]$. This was prepared in accordance with the literature.[29] Phosphotungstic acid hydrate (5.0 g, 1.74 mmol) was dissolved in water (20 mL). $(n\text{-}C_4H_9)_4NBr$ (TBABr) (1.67 g, 5.21 mmol) was dissolved in the phosphotungstic solution, under stirring for 1 h. The precipitate was collected, washed, and then dried with gentle heating producing a white crystalline powder (5.74 g, 85.9%).

Preparation of $Li_7[PW_{11}O_{39}]$. This was prepared in accordance with the adapted literature.[30] Phosphotungstic acid hydrate (5.0 g, 1.74 mmol) was dissolved in water (20 mL). LiCl (0.22 g, 5.21 mmol) was dissolved in the phosphotungstic solution. Aqueous solution of 1 M lithium hydrogencarbonate (6.79 g, 100 mL) was added dropwise until pH of the suspension reached pH 4.80. The crystalline salt was isolated by solvent evaporation and recrystallised from hot water. The crystals were dried with gentle heating producing a white crystalline powder (4.13 g, 87.1%).

Preparation of $Na_7[PW_{11}O_{39}]$. This was prepared in accordance with the adapted literature.[30] Phosphotungstic acid hydrate (5.0 g, 1.74 mmol) was dissolved in water (20 mL). NaCl (0.10 g, 5.21 mmol) was dissolved in the phosphotungstic solution. Aqueous solution of 1 M sodium hydrogencarbonate (8.40 g, 100 mL) was added dropwise until pH of the suspension reached pH 4.80. The crystalline salt was isolated by solvent evaporation and recrystallised from hot water. The crystals were dried with gentle heating producing a white crystalline powder (4.02 g, 81.4%).

Preparation of $K_7[PW_{11}O_{39}]$. This was prepared in accordance with the literature.[30] Phosphotungstic acid hydrate (25.0 g, 8.68 mmol) was dissolved in distilled water (100 mL). KCl (1.94 g, 26.04 mmol) was then added to the phosphotungstic solution. Aqueous solution of 1 M potassium hydrogencarbonate (10.01 g, 100 mL) was added dropwise until pH of the suspension reached pH 4.80. The filtrate was concentrated and allow to cool to room temperature. The white crystalline salt was recrystallised from hot water. The crystals were dried with gentle heating producing a white crystalline powder (24.70 g, 94.6%).

Preparation of $Na_8H[\Delta\text{-}PW_9O_{34}]$. This was prepared in accordance to the literature.[31] Sodium tungstate dihydrate (12.0 g) was dissolved in distilled water (14.8 mL) with stirring, then was added to 85% *ortho*-phosphoric acid (0.25 mL) followed by glacial acetic acid (2.2 ml). Gentle stirring produced a white precipitate which was isolated by filtration and washed for drying. The isomer was obtained depended on drying temperature. Drying between $20 < T < 80$ °C obtained $Na_8H[A\text{-}PW_9O_{34}]$, whilst at $T > 80$ °C, $Na_8H[B\text{-}PW_9O_{34}]$ isomer appeared in the product. Complete isomerism was conducted at $T = 140$ °C for several hours.

Computational details

All computational results were obtained using the ARCHIE-WeSt High-Performance Computer based at the University of Strathclyde. Density Functional Theory (DFT) cal-

culations were performed using the Amsterdam Modelling Suite (AMS 2020.1) package.[32] In this work, two classes of exchange–correlation (*x*–*c*) functionals were employed, which include: (i) generalized gradient approximation (GGA); (ii) and hybrid methodologies. GGA functionals considered were Perdew–Burke–Ernzerhof (PBE).[33] The hybrid *x*–*c* functionals considered were: (i) Becke, 3-parameter, Lee–Yang–Parr (B3LYP*,[34] B3LYP[35]); (ii) Perdew–Burke–Ernzerhof (PBE0);[36] (iii) and Becke's half-and-half (BH&H).[37] Hybrid functionals were selected on their contributions of Hartree–Fock (HF) exchange (15% B3LYP*, 20% B3LYP, 25% PBE0, and 50% BH&H). We employed Slater basis sets comprising: (i) triple-ζ polarization (TZP); (ii) triple-ζ plus polarization (TZ2P); (iii) and quadruple-ζ plus polarization (QZ4P).[38,39] Relativistic corrections were included by means of the zeroth order regular approximation (ZORA) formalism.[40] The effects of aqueous solvent were approximated by using the conductor-like screening model (COSMO), as implemented by AMS.[41]

^{31}P-NMR signals were computed using several *x*–*c* functionals with varying degrees of HF exchange (0% PBE, 15% B3LYP*, 20% B3LYP, 25% PBE0, 50% BH&H). Also, the effect of larger basis sets (TZ2P & QZ4P) was investigated, restricted to the GGA–PBE level of theory. Relativistic corrections were included by the zeroth order regular approximation (ZORA) formalism and the aqueous solution was approximated by using the conductor-like screening model (COSMO), as implemented by AMS. Thereafter, single-point calculations were employed to calculate ^{31}P-NMR parameters (hyperfine couplings and isotropic shielding constants) with spin–orbit (SO) corrections. The notation for this procedure is expressed throughout the text as Functional^{NMR}/Basis^{NMR}//Functional^{OPT}/Basis^{OPT}. Herein, all ^{31}P NMR calculations were performed using PBE/TZP. The chemical shifts were referenced to 85% H_3PO_4 using PH_3 as a secondary standard following the method suggested by van Wüllen:[42]

$$\delta(X_{Calc}) = \sigma(PH_{3Calc}) - \sigma(X_{Calc}) - 266.1 \quad (1)$$

where X is the phosphorus atom in the model system of interest and 266.1 is the difference in ppm between the absolute experimental chemical shielding of PH_3 (594.5 ppm) and 85% H_3PO_4 (328.4 ppm) at 300 K.[43] The use of a secondary standard for ^{31}P has become a frequent model of choice, as the theoretical chemical shielding for 85% H_3PO_4 is difficult to obtain.[44]

The chemical shift of a nucleus is dependent on the magnetic shielding tensor, σ. The shielding tensor can be rewritten in terms of the diamagnetic, paramagnetic, and spin–orbit contributions, see below:

$$\sigma = \sigma^{d} + \sigma^{p} + \sigma^{SO} \quad (2)$$

σ_d corresponds to the diamagnetic tensor which depends on the electron density at the ground state. σ_p equates to the paramagnetic tensor which depends on the excited states of the unperturbed system. Conventionally, σ_d is analogous across chemical environments so changes in chemical shift is usually attributed to the paramagnetic part. The paramagnetic tensor can be expressed as:

$$u_{ai} \propto -\frac{\Psi_a|\hat{M}|\Psi_i}{2(\varepsilon_i^0 - \varepsilon_a^0)} \quad (3)$$

where ε_i^0 and ε_a^0 are the orbital energies of the occupied and unoccupied MOs involved in a given electronic transition, and the integral in the numerator is the first-order magnetic coupling between these orbitals.

Finally, to evaluate the discrepancy of the calculated *vs.* experimental chemical shifts, we employed the mean unassigned error (MUE), the mean signed error (MSE) obtained as:

$$MAE = \frac{1}{N}\sum_i \left|\delta_{Calc,i} - \delta_{exp,i}\right| \quad (4)$$

$$MSE = \frac{1}{N}\sum_i \left(\delta_{Calc,i} - \delta_{exp,i}\right) \quad (5)$$

$$STD = \sqrt{\frac{1}{N-1}\sum_i \left(MSE - \left(\delta_{Calc,i} - \delta_{Exp,i}\right)\right)^2} \quad (6)$$

where δ_{Calc} and δ_{exp} are the calculated and experimental chemical shifts, respectively.

Results and discussion

Anionic model

In this section, we seek to establish an optimal computational practise for calculating ^{31}P NMR signals by using several *x*–*c* functionals with varying contributions of exact Hartree–Fock (HF) exchange (0% PBE, 15% B3LYP*, 20% B3LYP, 25% PBE0, 50% BH&H). The influence of applied basis set (TZ2P & QZ4P) was restricted to the GGA–PBE functional. Our initial work focussed on anionic systems, shown in Fig. 3.

Computed $\delta(^{31}P)$ signals for Keggin, $[PW_{12}O_{40}]^{3-}$ and their corresponding lacunary: $[PW_{11}O_{39}]^{7-}$, $[A\text{-}PW_9O_{34}]^{9-}$, and $[B\text{-}PW_9O_{34}]^{9-}$ clusters are presented in Fig. 3. $\delta_{Calc}(^{31}P)$ for Keggin, $[PW_{12}O_{40}]^{3-}$, were reproduced within *ca.* 8 ppm across all methods with respect to the experimental, $\delta_{exp}(^{31}P)$ – see Table 1. $\delta_{Calc}(^{31}P)$ for anionic Keggin systems, $[PW_{12}O_{40}]^{3-}$ were in closer agreement with $\delta_{exp}(^{31}P)$ of $Na_3[PW_{12}O_{40}]$. The discrepancy between $\delta_{Calc}(^{31}P)$ and $\delta_{Exp}(^{31}P)$ was represented by $\delta_{Error}(^{31}P)$. Herein, $\delta_{Error}(^{31}P)$ decreased as a function of exact Hartree–Fock (HF) exchange which was attributed shortening of P–O distances. For example, as exchange was increased from 15% (B3LYP*) to 50% (BH&H), P–O in $[PW_{12}O_{40}]^{3-}$ decreased by 0.026 Å, reflecting in the range of 7.87 ppm. All computed entries for $[PW_{12}O_{40}]^{3-}$ produced P–O geometries in the region of 1.519–1.545 Å, closely replicating the crystallographic structure of 1.530 Å.[45]

Computed chemical shifts, $\delta_{Calc}(^{31}P)$, will be rationalised as a function of structural geometry. The magnetic shielding tensor, σ, is comprised of the sum of three contributions: (i) diamagnetic; (ii) paramagnetic; (iii) and the spin–orbit (SO) correction – see

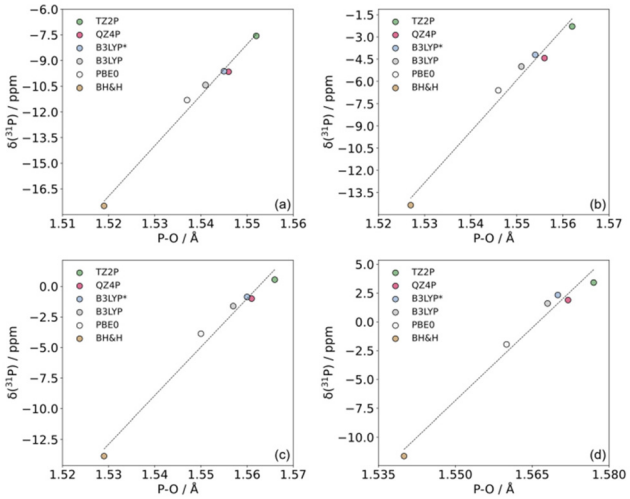

Fig. 3 Computed chemical shift, $\delta_{Calc}(^{31}P)$, plotted as a function of P–O distance for the hydrolytic conversions of (a) $[PW_{12}O_{40}]^{3-}$ to lacunary: (b) $[PW_{11}O_{39}]^{7-}$, (c) $[A\text{-}PW_9O_{34}]^{9-}$, and (d) $[B\text{-}PW_9O_{34}]^{9-}$ clusters. Optimisations were performed *x–c* functionals with varying degrees of Hartree–Fock (HF) exchange (0% PBE–50% BH&H). All NMR calculations were performed using PBE/TZP.

eqn (2). The diamagnetic contribution to shielding is dominated by core orbitals contributions which are largely unaffected by the chemical environment. Hence, $\delta_{Calc}(^{31}P)$ can be attributed to the paramagnetic term, σ_p. eqn (3) shows the principal contributor to the paramagnetic term is u_{ai}, which depends on the reciprocal of the energy gap between the occupied and virtual orbitals involved in transition. HOMO LUMO gaps are not the same as transitions atttributed to the P nucleus!

Generally, employment of hybrid *x–c* functionals proved superior and were in closer agreement with $\delta_{exp}(^{31}P)$ with respect to GGA-PBE coupled with triple-ζ plus polarization (TZ2P) or quadruple-ζ plus polarization (QZ4P) basis sets. This observation was attributed to an over-expansion of the PO_4 tetrahedron. Our computed signals shown an inverse correlation with Hartree–Fock (HF) exchange, shown in Fig. 3. The contraction of the PO_4 tetrahedron induced shielding of the nucleus. Consequently, the energy gap between the occupied and virtual orbitals involved in transition have increased with contraction of the P–O distances. One would expect that for small energy gaps, this will reinforce σ_p (more negative), and the shielding tensor, σ, becomes less positive, displacing $\delta_{Calc}(^{31}P)$ to more positive regions. Hence, the energy gap between the occupied and virtual orbitals increases and u_{ai} becomes less negative.

Incorporation of alkali metal cations

In this work, we have explicitly located alkali metal (X = Li^+, Na^+, K^+) cations to render our systems charge neutral. On the surface of the molecule, the counterion can interact with 4-fold (pocket A–F) or 3-fold pockets – see Fig. S9.†[14] The 4-fold pockets feature four oxygen atoms capable of interacting with counterions, whilst 3-fold pockets are comprised of three adjacent oxygen atoms which assume a triangular shape. In our previous work, we established alkal-.metal counterions preferentially interact with the 4-fold pockets because of improved Coulomb interactions.[14] Herein, we have explicitly located alkali metal (X = Li^+, Na^+, K^+) cations into 4-fold hollow sites, unless specified otherwise, to render the system neutral.

Computed $\delta(^{31}P)$ signals for Keggin, $X_3[PW_{12}O_{40}]$ and their corresponding lacunary: $X_7[PW_{11}O_{39}]$, $X_9[A\text{-}PW_9O_{34}]$, and $X_9[B\text{-}PW_9O_{34}]$ (X = Li^+, Na^+, K^+, TBA^+) clusters are presented in Table 1. Incorporation of counterions to $[PW_{12}O_{40}]^{3-}$ induced (minimal) deshielding by approx. 0.5–1.5 ppm. The active nuclei in $X_3[PW_{12}O_{40}]$ (X = Li^+, Na^+) became more shielded (0.3 –

Table 1 Computed $\delta_{Calc}(^{31}P)$ signals for Keggin, $[PW_{12}O_{40}]^{3-}$ and their corresponding lacunary: $[PW_{11}O_{39}]^{7-}$, $[A\text{-}PW_9O_{34}]^{9-}$ with $[B\text{-}PW_9O_{34}]^{9-}$ clusters and their corresponding salts (X = Li^+, Na^+, K^+, TBA^+). All NMR calculations were performed as single point calculations using PBE/TZP with spin orbit correction (SO-ZORA).

PBE^{NMR}/TZP^{NMR}// $Functional^{OPT}/Basis^{OPT}$	$\delta_{Calculated}(^{31}P)$						$\delta_{Experimental}(^{31}P)$	
	PBE/TZ2P	PBE/QZ4P	B3LYP*/TZP	B3LYP/TZP	PBE0/TZP	BH&H/TZP	**Our work**	Lit.[19,46]
$[\mathbf{PW_{12}}O_{40}]^{3-}/H_2O$	−7.56	−9.66	−9.63	−10.43	−11.30	−17.50		−14.60[a]
$Li_3[PW_{12}O_{40}]$	−7.90 (7.5)	−10.22 (5.2)	−10.27 (5.1)	−11.03 (4.4)	−12.84 (2.6)	−18.55 (3.1)	**−15.41**	
$Na_3[PW_{12}O_{40}]$	−8.28 (7.1)	−10.80 (4.6)	−10.65 (4.7)	−11.39 (4.0)	−13.04 (2.3)	−19.04 (3.7)	**−15.36**	
$[PW_{12}O_{40}]^{3-}$/MeCN	−7.55	−9.62	−9.27	−9.97	−11.38	−17.50		
$TBA_3[PW_{12}O_{40}]$	−8.25 (7.1)	−11.40 (4.0)	−9.75 (5.6)	−10.68 (4.7)	−12.33 (3.0)	−19.65 (4.3)	**−15.35**	
$[\mathbf{PW_{11}}O_{39}]^{7-}/H_2O$	−2.29	−4.43	−4.21	−5.00	−6.59	−14.35		
$Li_7[PW_{11}O_{39}]$	−3.47 (8.2)	−5.38 (6.3)	−5.35 (6.3)	−6.16 (5.5)	−7.27 (4.4)	−14.92 (3.5)	**−11.65**	−11.20
$Na_7[PW_{11}O_{39}]$	−2.33 (8.5)	−4.65 (6.2)	−4.58 (6.2)	−5.37 (5.5)	−7.35 (3.5)	−14.28 (3.5)	**−10.82**	−10.65
$K_7[PW_{11}O_{39}]$	−3.40 (7.7)	−6.06 (5.1)	−6.05 (5.1)	−6.82 (4.3)	−8.5 (2.6)	−16.28 (5.2)	**−11.13**	−10.80
$[A\text{-}\mathbf{PW_9}O_{34}]^{9-}/H_2O$	0.55	−1.00	−0.86	−1.61	−3.87	−13.86		
$Na_8H[A\text{-}PW_9O_{34}]$	−0.99 (6.8)	−2.34 (5.4)	−2.39 (5.4)	−3.24 (4.5)	−5.10 (2.7)	−12.83 (5.1)	**−7.76**	−7.10
$[B\text{-}\mathbf{PW_9}O_{34}]^{9-}/H_2O$	3.41	1.89	2.33	1.60	−1.96	−11.64		
$Na_8H[B\text{-}PW_9O_{34}]$	11.05 (14.8)	9.23 (13.0)	9.17 (12.9)	8.15 (11.9)	6.28 (2.5)	−2.96 (0.8)	**−3.76**	−3.00
MAE	8.65	6.37	6.61	5.79	4.03	3.74		
MSE	8.65	6.37	6.61	5.79	4.03	−3.54		
STD	2.54	2.83	2.66	2.58	2.53	1.57		

[a] Protonated species. (Value) Discrepancy values in parentheses calculated using: $\delta_{Exp}(^{31}P)$ minus $\delta_{Calc}(^{31}P)$.

0.5 ppm) as the ionic radii of alkali–metal cation was increased from ca. 2.125 to 2.250 Å ($Li^+$to Na^+). $\delta_{Calc}(^{31}P)$ calculated using PBE0/TZP produced the strongest agreement with $\delta_{Exp}(^{31}P)$ shifted upfield by 2.5 ppm, relative to experimental data.

The accuracy of *x–c* functionals was assessed, in which, increasing HF exchange progressively shifted signals upfield from −10.27 (15% B3LYP*) to −18.55 ppm (50% BH&H) in $Li_3[PW_{12}O_{40}]^{3-}$ salts and −10.80 (15% B3LYP*) to −19.04 ppm (50% BH&H) in $Na_3[PW_{12}O_{40}]$, salts. Negligible effects to $\delta(^{31}P)$ were induced by changing the implicit solvent (H_2O → MeCN) shown for $[PW_{12}O_{40}]^{3-}$ in which $\Delta\delta(^{31}P)$ did not exceed 0.5 ppm.

Assessment of the lacunary, $X_7[PW_{11}O_{39}]$ (X = Li^+, Na^+) clusters were shifted downfield by 4.0–5.0 ppm with respect to Keggin, $X_3[PW_{12}O_{40}]$. $\delta(^{31}P)$ signal in $Na_7[PW_{11}O_{39}]$ clusters were shifted upfield by 1.0–1.5 ppm, with respect to $Li_7[PW_{11}O_{39}]$ clusters. Conversely, $\delta(^{31}P)$ signals in $K_7[PW_{11}O_{39}]$ clusters were shifted downfield by *ca.* 1.0 ppm relative to $Na_7[PW_{11}O_{39}]$ revealing the overall trend: K^+ (upfield) > Li^+ > Na^+ (downfield). Unfortunately, our computational model is unable to replicate the order of $\delta_{Exp}(^{31}P)$ values in $X_7[PW_{11}O_{39}]$: Li^+ (upfield) > K^+ > Na^+ (downfield). This is probably since our model overlooks the ion pairing effect in aqueous solutions of polyoxometalate anions with different cations. In 2008 Poblet and co-workers studied the delicate interplay between electrostatic interactions and the proximity effect in the aqueous solutions of three different POMs, $[PW_{12}O_{40}]^{3-}$, $[SiW_{12}O_{40}]^{4-}$, and $[AlW_{12}O_{40}]^{5-}$, with respect to three different monovalent cations Li^+, Na^+, and K^+.[47] Later , Nyman and co-workers successfully investigated the ion-pairing effect in Mo– based Lindqvist($[(CH_3)_4N]^+$,$Cs)_8[M_6O_{19}]$ (M = Nb, Ta), combining experiments and theory. Their system is particularly challenging as the clusters water solubility increases with stronger ion-pairing, contrary to most ionic salts.[48] Although, the best overall computational methodology was not consistent across the lacunary clusters. The influence of exact exchange progressively shielded $\delta(^{31}P)$ values, for example: from −5.35 (15% B3LYP*) to −14.92 ppm (50% BH&H) in $Li_7[PW_{11}O_{39}]$, salts. Generally, optimisations using PBE0/TZP (20% exchange) accurately replicated the experimental, reporting a mean absolute error (MAE) of 4.03 ppm. Computation with BH&H/TZP demonstrated the lowest value of MAE (3.74 ppm), attributed to an excellent replication of $\delta(^{31}P)$ in $Na_8H[B\text{-}PW_9O_{34}]$.

Incorporation of alkylammonium cations

To further this work, we have explicitly incorporated alkylammonium cations, neutralising our systems to: $[(n\text{-}C_xH_{2x+1})_4N]_3[PW_{12}O_{40}]$; where x = 1–4 (Table 2). The alkylammonium cations adopted a triangular arrangement around the Keggin, $[PW_{12}O_{40}]^{3-}$ in which the central heteroatom is coplanar with the cations, see Fig. S10.†

The arrangement of $[(n\text{-}C_xH_{2x+1})_4N]_3$ can be assessed by the average central heteroatom (P) – nitrogen (ammonium) distance calculated at 5.601, 7.227, 8.003, 7.919, and 8.043 Å for NH_4^+, n-$(CH_3)_4^+$, n-$(C_2H_5)_4^+$, n-$(C_3H_7)_4^+$, and n-$(C_4H_9)_4^+$, respectively. Optimizations using PBE0/TZP for $[(n\text{-}C_4H_9)_4N]_3[PW_{12}O_{40}]$ produced $\delta(^{31}P)$ with reasonable agreement with the experimental (*ca.* 3.0 ppm). However, optimizations of $[(n\text{-}C_xH_{2x+1})_4N]_3[PW_{12}O_{40}]$ (x = 3 or 4) with hybrid *x–c* functionals is CPU expensive, hence, we explored the sensitivity of $\delta(^{31}P)$ of alkyl chain length in $[(n\text{-}C_xH_{2x+1})_4N]_3$. Computed $\delta_{Calc}(^{31}P)$ was shielded by 0.67 ppm from −12.33 ($[(n\text{-}C_4H_9)_4N]^+$) to −13.00 ($[NH_4]^+$). Interestingly, optimisations using $[NH_4]^+$ cations yielded the closest agreement with the experimental values.

Table 2 Computed, $\delta_{Calc}(^{31}P)$ for alkyl ammonium Keggin, $[(n\text{-}C_xH_{2x+1})_4N]_3[PW_{12}O_{40}]$ salts, reported in ppm. The difference in, $\delta_{Calc}(^{31}P)$ relative to $[(n\text{-}C_4H_9)_4N]_3[PW_{12}O_{40}]$ is represented by $\Delta\delta_{Calc}(^{31}P)$. Optimizations were performed using PBE0/TZP level of theory. All NMR calculations were performed using PBE/TZP

$[(n\text{-}C_xH_{2x+1})_4N]^+$	$\delta_{Calc}(^{31}P)$	$\Delta\delta_{Calc}(^{31}P)$
$[NH_4]^+$	−13.00	0.67
$[(n\text{-}CH_3)_4N]^+$	−12.68	0.35
$[(n\text{-}C_2H_5)_4N]^+$	−12.70	0.37
$[(n\text{-}C_3H_7)_4N]^+$	−12.83	0.50
$[(n\text{-}C_4H_9)_4N]^+$	−12.33	0.00

Empirical scaling was performed to correct the discrepancies between the computed and experimental work. The present work employed data points obtained using the PBE/TZP//PBE0/TZP methodology, thereby computed isotropic shielding (σ) was plotted taking the form $\delta = b\sigma + a$, in which the slope, b, is the scaling factor, see Fig. 4. Table S2† reports the comparison between experimental, δ_{Exp}, computed, δ_{Comp}, and fitted, δ_{Fitted}, chemical shifts (Fig. 5).

The fitted values, $\delta_{Fitted}(^{31}P)$, revealed significantly lower MAE values of 0.86 and were not systematically underestimated shown by MSE of −0.02 ppm. $\delta_{Fitted}(^{31}P)$ replicated the order of $\delta(^{31}P)$ values in $X_7[PW_{11}O_{39}]$ (X = Li^+, Na^+, K^+) replicating the experimental within *ca.* 0.9 ppm, see Fig. 4 and Table S2.† A significant improvement for the tri-lacunary: $Na_8H[A\text{-}PW_9O_{34}]$ and $Na_8H[B\text{-}PW_9O_{34}]$ clusters were observed, in which $\delta_{Error}(^{31}P)$ was reduced from 2.66 and 10.04 using PBE/TZP//PBE0/TZP to 2.11 and 1.04 using fitted values, $\delta_{Fitted}(^{31}P)$. Computed $\delta(^{31}P)$ signals for $Na_8H[B\text{-}PW_9O_{34}]$ were challenging to accurately compute without correctional fitting. No correlation between ion-pair

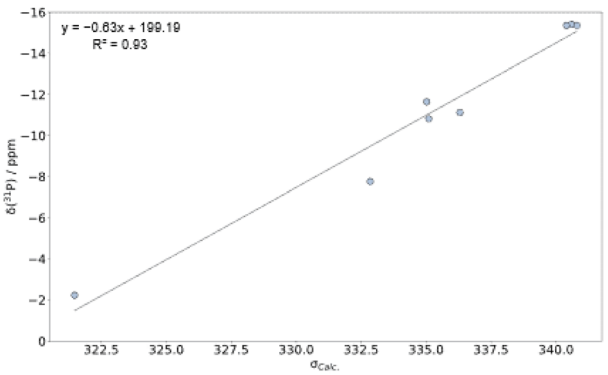

Fig. 4 Computed isotropic shielding, σ_{Calc} using the PBE/TZP//PBE0/TZP methodology, plotted as a function of experimental $\delta_{Exp}(^{31}P)$ values.

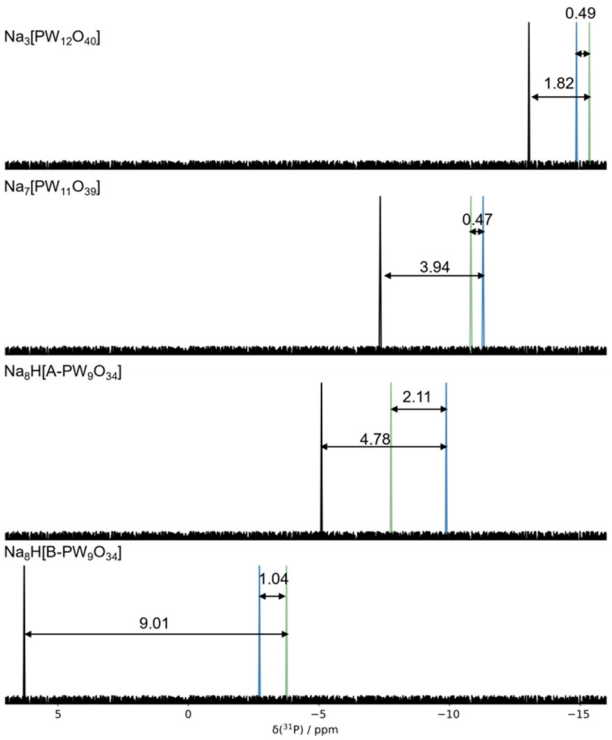

Fig. 5 Computed (black), $\delta_{Exp}(^{31}P)$, fitted (blue), $\delta_{Fitted}(^{31}P)$, and experimental (green), $\delta_{Exp}(^{31}P)$, signals for Keggin, $Na_3[PW_{12}O_{40}]$ and their corresponding lacunary: $Na_7[PW_{11}O_{39}]$, $Na_9[A\text{-}PW_9O_{34}]$, and $Na_9[B\text{-}PW_9O_{34}]$ clusters. All NMR calculations were performed using PBE/TZP.

proximity and chemical shift was observed, contrasted to redox potentials shown in our previous work. The effect of the functional outweighs the effect of the counterions.

Conclusions

In this work, we have employed Density Functional Theory (DFT) calculations to systematically study the accuracy of exchange– correlation functionals and applied basis sets for reproducing experimental chemical shift, $\delta_{Exp}(^{31}P)$ values. Our objective has been to establish a methodology for obtaining accurate $\delta_{Calc}(^{31}P)$ signals in Keggin-based clusters and to provide an insight into the geometric factors controlling it.

Computation of $\delta_{Exp}(^{31}P)$ for Keggin, $[PW_{12}O_{40}]^{3-}$, were in closer agreement to $\delta_{Calc}(^{31}P)$ obtained for $Na_3[PW_{12}O_{40}]$. Generally, discrepancies between $\delta_{Calc}(^{31}P)$ and $\delta_{Exp}(^{31}P)$ represented by $\delta_{Error}(^{31}P)$ decreased as a function of Hartree–Fock (HF) exchange, attributed to shortening of P–O. Explicitly located counterions reduced discrepancies by 1.0–2.0 ppm across all Keggin and corresponding lacunary compounds which was attributed to their deshielding effect. However, obtaining accurate approximations for for $[B\text{-}PW_9O_{34}]^{9-}$ remains a challenge due to direct electrostatic interactions between the located counterions and central tetrahedron. Optimal results were achieved using the PBE/TZP//PBE0/TZP method, achieving an MAE and MSE of 4.03 ppm. Linear scaling was performed to reduce discrepancies between the computed and experimental work,in which $\delta_{Fitted}(^{31}P)$, revealed lower MAE values of 0.86 ppm and were not systematically underestimated shown by MSE of −0.02 ppm.

Data availability

The datasets generated using DFT calculations are available in the ioChem-BD database: **https://iochem-bd.bsc.es/browse/handle/100/312985**

Author contributions

L.V.-N. conceived the idea together with J. A. T. who designed the modelling approach, performed all calculations, synthesised, and fully characterised all the compounds and analysed all the data. J. A. T. wrote the paper and made all tables and figures in the manuscript with input from L.V.-N.

Conflicts of interest

There are no conflicts to declare.

Acknowledgements

Financial support for this work was provided by University of Glasgow and the Engineering and Physical Sciences Research Council Grants (EP/S030603/1; EP/V048341/1; EP/S031170/1), Royal Society of Chemistry RSC Hardship Grant (COVID-19). We thank the EPSRC Doctoral Training Partnership (DTP) funding received by the University of Glasgow for Jake A. Thompson PhD studentship 'Exploring N_2 fixation with metal oxides' project 2442596 (EP/R513222/1; EP/T517896/1). We also thank the University of Glasgow (UofGla) Early Career Development Programme (ECDP) 2021, the UofGla Reinvigorating Research Scheme 2022, and the School of Chemistry for long-lasting support. We thank ScotCHEM for 2022 ECR equipment funding and we also thank the Cronin Group for upcylced glassware and equipment. Finally, we thank Mr Alec Mungall, for help collecting NMR samples, and all the technical staff in the School of Chemistry for support during this work. Results were obtained using the ARCHIE-WeSt High-Performance Computer (**https://www.archie-west.ac.uk**) based at the University of Strathclyde.

References

1 A. V. Anyushin, A. Kondinski and T. N. Parac-Vogt, *Chem. Soc. Rev.*, 2020, **49**, 382–432.
2 N. I. Gumerova and A. Rompel, *Chem. Soc. Rev.*, 2020, **49**, 7568–7601.

3 N. V. Izarova, M. T. Pope and U. Kortz, *Angew. Chem., Int. Ed.*, 2012, **51**, 9492–9510.
4 A. Proust, B. Matt, R. Villanneau, G. Guillemot, P. Gouzerh and G. Izzet, *Chem. Soc. Rev.*, 2012, **41**, 7605–7622.
5 A. S. Cherevan, S. P. Nandan, I. Roger, R. Liu, C. Streb and D. Eder, *Adv. Sci.*, 2020, **7**, 1903511.
6 S. M. Wilson, B. E. Petel, E. Schreiber, M. L. Maiola, P. Su, E. M. Matson and J. Laskin, *Chem. – Eur. J.*, 2023, **29**, 1–10.
7 C. P. Pradeep, D. L. Long and L. Cronin, *J. Chem. Soc., Dalton Trans.*, 2010, **39**, 9443–9457.
8 M. S. Balulla, J. A. Gamelas, H. M. Carapuça, A. M. V. Cavaleiro and W. Schlindwein, *Eur. J. Inorg. Chem.*, 2004, 619–628.
9 A. Misra, K. Kozma, C. Streb and M. Nyman, *Angew. Chem., Int. Ed.*, 2020, **59**, 596–612.
10 D.-L. Long, E. Burkholder and L. Cronin, *Chem. Soc. Rev.*, 2007, **36**, 105–121.
11 H. N. Miras, L. Vilà-Nadal and L. Cronin, *Chem. Soc. Rev.*, 2014, **43**, 5679–5699.
12 S. Khlifi, J. Marrot, M. Haouas, W. E. Shepard, C. Falaise and E. Cadot, *J. Am. Chem. Soc.*, 2022, **144**, 4469–4477.
13 S. Azuma, T. Kadoguchi, Y. Eguchi, H. Hirabaru, H. Ota, M. Sadakane, K. Yanagisawa, T. Hasegawa and T. Ueda, *Dalton Trans.*, 2020, **49**, 2766–2770.
14 J. A. Thompson, R. González-Cabaleiro and L. Vilà-Nadal, *Inorg. Chem.*, 2023, **62**, 12260–12271.
15 D. Laurencin, R. Thouvenot, K. Boubekeur, P. Gouzerh and A. Proust, *C. R. Chim.*, 2012, **15**, 135–142.
16 M. Sadakane, D. Tsukuma, M. H. Dickman, B. Bassil, U. Kortz, M. Higashijima and W. Ueda, *Dalton Trans.*, 2006, 4271–4276.
17 P. Klonowski, J. C. Goloboy, F. J. Uribe-Romo, F. Sun, L. Zhu, F. Gándara, C. Wills, R. J. Errington, O. M. Yaghi and W. G. Klemperer, *Inorg. Chem.*, 2014, **53**, 13239–13246.
18 R. González-Cabaleiro, J. A. Thompson and L. Vilà-Nadal, *Front. Chem.*, 2021, **9**, 742565.
19 R. I. Maksimovskaya and G. M. Maksimov, *Coord. Chem. Rev.*, 2019, **385**, 81–99.
20 L. Vilà-Nadal and L. Cronin, *Nat. Rev. Mater.*, 2017, **2**, 17054.
21 R. Contant and A. Tézé, *Inorg. Chem.*, 1985, **24**, 4610–4614.
22 A. Bagno and M. Bonchio, *Eur. J. Inorg. Chem.*, 2002, 1475–1483.
23 (*a*) A. Bagno, M. Bonchio, A. Sartorel and G. Scorrano, *Eur. J. Inorg. Chem.*, 2000, 17–20; (*b*) A. Bagno, M. Bonchio, A. Sartorel and G. Scorrano, *ChemPhysChem*, 2003, **4**, 517–519; (*c*) A. Bagno, M. Bonchio and J. Autschbach, *Chem. – Eur. J.*, 2006, **12**, 8460–8471.
24 N. Vankova, T. Heine and U. Kortz, *Eur. J. Inorg. Chem.*, 2009, 5102–5108.
25 L. Vilà-Nadal, J. P. Sarasa, A. Rodríguez-Fortea, J. Igual, L. P. Kazansky and J. M. Poblet, *Chem. – Asian J.*, 2010, **5**, 97–104.
26 M. Pascual-Borràs, X. López, A. Rodríguez-Fortea, R. J. Errington and J. M. Poblet, *Chem. Sci.*, 2014, **5**, 2031–2042.
27 M. Pascual-Borràs, X. López and J. M. Poblet, *Phys. Chem. Chem. Phys.*, 2015, **17**, 8723–8731.
28 J. A. Dias, S. C. L. Dias, E. Caliman, J. Bartis and L. Francesconi, Keggin Structure Polyoxometalates, *Inorg. Synth.*, 2014, **36**, 210–217.
29 J. A. Gamelas, F. A. S. Couto, M. C. N. Trovão, A. M. V. Cavaleiro, J. A. S. Cavaleiro and J. D. P. de Jesus, *Thermochim. Acta*, 1999, **326**, 165–173.
30 N. Haraguchi, Y. Okaue, T. Isobe and Y. Matsuda, *Inorg. Chem.*, 1994, **33**, 1015–1020.
31 B. Moore and K. Foger, *Inorg. Chim. Acta*, 1991, **181**, 201–205.
32 G. te Velde, F. M. Bickelhaupt, E. J. Baerends, C. Fonseca Guerra, S. J. A. van Gisbergen, J. G. Snijders and T. Ziegler, *J. Comput. Chem.*, 2001, **22**, 931–967.
33 J. P. Perdew, K. Burke and M. Ernzerhof, *Phys. Rev. Lett.*, 1997, **78**, 3865–3868.
34 M. Reiher, O. Salomon and B. A. Hess, *Theor. Chem. Acc.*, 2001, **107**, 48–55.
35 C. Lee, E. Yang and R. G. Parr, *Phys. Rev. B: Condens. Matter Mater. Phys.*, 1998, **37**, 785.
36 M. Ernzerhof and G. E. Scuseria, *J. Chem. Phys.*, 1999, **110**, 5029–5036.
37 A. D. Becke, *J. Chem. Phys.*, 1993, **98**, 1372–1377.
38 R. Sure, J. G. Brandenburg and S. Grimme, *ChemistryOpen*, 2016, **5**, 94–109.
39 E. Van Lenthe and E. J. Baerends, *J. Comput. Chem.*, 2003, **24**, 1142–1156.
40 E. Van Lenthe, *J. Chem. Phys.*, 1999, **110**, 8943–8953.
41 C. C. Pye and T. Ziegler, *Theor. Chem. Acc.*, 1999, **101**, 396–408.
42 C. Van Wüllen, *Phys. Chem. Chem. Phys.*, 2000, **2**, 2137–2144.
43 D. B. Chesnut, *J. Phys. Chem. A*, 2005, **109**, 11962–11966.
44 J. Přecechtělová, P. Novák, M. L. Munzarová, M. Kaupp and V. Sklenář, *J. Am. Chem. Soc.*, 2010, **132**, 17139–17148.
45 G. M. Brown, M.-R. Noe-Spirlet, W. R. Busing and H. A. Levy, *Acta Crystallogr.*, 1977, 1038–1046.
46 M. Kozik, C. F. Hammer and L. C. W. Baker, *J. Am. Chem. Soc.*, 1986, **108**, 7627–7630.
47 F. Leroy, P. Miró, J. M. Poblet, C. Bo and J. Bonet-Ávalos, *J. Phys. Chem. B*, 2008, **112**(29), 8591–8599.
48 J. Sures, S. A. Serapian, K. Kozma, P. I. Molina, C. Bo and M. Nyman, *Phys. Chem. Chem. Phys.*, 2017, **19**, 8715–8725D.